Sensing and Bio-Sensing Research 45 (2024) 100670

Contents lists available at ScienceDirect

Sensing and Bio-Sensing Research

journal homepage: www.elsevier.com/locate/sbsr

Gold nanowire-infused square-clad SPR-PCF biosensor for detection of various cancer cells

Atiqul Alam Chowdhury [a], Md Rezaul Hoque Khan [a,*], Mohammad Rakibul Islam [a], A.N.M. Iftekher [a], Md Sanowar Hosen [a,b], Mhamud Hasan Mim [a], Mirza Muntasir Nishat [a]

[a] Department of Electrical & Electronics Engineering, Islamic University of Technology, Dhaka, Bangladesh
[b] Department of Electrical & Electronics Engineering, Daffodil International University, Daffodil Smart City, Ashulia, Dhaka, Bangladesh

ARTICLE INFO

Keywords:
Biosensor
SPR-PCF
cancer cell
Confinement loss
Wavelength sensitivity
Amplitude sensitivity
Resolution

ABSTRACT

This research work introduces a Surface Plasmon Resonance (SPR) based Photonic Crystal Fiber (PCF) sensor using gold nanowires as plasmonic material designed for the detection of various cancer cells, boasting remarkable sensitivity and ease of fabrication. The sensor's structure was devised and analyzed using the Finite Element Method (FEM) of COMSOL v5.5, with a focus on exploring the impact of varying geometric parameters on its overall performance. The simulation utilized extremely fine mesh elements to ensure the utmost accuracy. Excitation between the core and plasmonic modes is achieved using Gold (Au) nanowires. The determination of the sensor's wavelength sensitivity involves assessing the resonance wavelength shift between samples of normal and cancerous cells. Simultaneously, the measurement of amplitude sensitivity is accomplished through a comparison of the amplitudes associated with their respective confinement losses. Various parameters of the PCF were varied during the experimentation, leading to the achievement of exceptionally high Amplitude Sensitivity (AS) of -273.16 RIU^{-1}, -286.58 RIU^{-1}, -455.59 RIU^{-1}, -698.76 RIU^{-1}, -1172.72 RIU^{-1} and -1971.30 RIU^{-1} for Skin Cancer, Cervical Cancer, Blood Cancer, Adrenal Gland Cancer, Breast Type-1 Cancer and Breast Type-2 Cancer respectively. Additionally, the Wavelength Sensitivity (WS) values were found to be 6500 nm/RIU, 14583.33 nm/RIU, 16428.57 nm/RIU, 25714.28 nm/RIU, 32857.14 nm/RIU, and 35714.28 nm/RIU for the same cancer types, respectively. The achieved resolutions for wavelength sensitivity are 1.54×10^{-5} RIU, 6.86×10^{-6} RIU, 6.09×10^{-6} RIU, 3.89×10^{-6} RIU, 3.04×10^{-6} RIU and 2.80×10^{-6} RIU, while the resolutions for amplitude sensitivity are 7.32×10^{-5} RIU, 8.37×10^{-5} RIU, 3.07×10^{-5} RIU, 2.00×10^{-5} RIU, 1.19×10^{-5} RIU and 7.10×10^{-6} RIU for the respective cancer types mentioned above. The design of the presented biosensor is notably uncomplicated and can be readily manufactured using contemporary fabrication techniques. In summary, the remarkable sensitivity exhibited by the proposed SPR-based PCF (SPR-PCF) biosensor, shows significant potential for enhancing the detection of cancer cells.

1. Introduction

Optical sensors are crucial in modern detection and measurement technologies. Optical sensors stand out as particularly remarkable innovations in sensing applications [1–8]. Optical sensors exploit the interaction between light and the target analyte to distinguish among various substances [9]. Their high sensitivity, fast response time and ability to provide real-time, non-contact measurements make them invaluable in various applications, including medical diagnostics, environmental monitoring and industrial automation. By detecting subtle changes in light properties, optical sensors can measure parameters such as temperature, pressure and refractive index with remarkable precision. Owing to their many benefits, optical sensors have attracted a lot of interest and have been widely used. Due to their elevated specificity and sensitivity, optical sensors are recognized for delivering high accuracy. In addition, their affordability and compact size make them perfect for a range of uses [9–11]. One of the most significant advancements in optical sensing technology is the development of Surface Plasmon Resonance (SPR) sensors. SPR sensors operate by measuring changes in the refractive index at the interface between a metal and a dielectric material. This makes them exceptionally sensitive to molecular interactions, allowing for the detection of biomolecules,

* Corresponding author.
E-mail address: rhkhan@iut-dhaka.edu (M.R.H. Khan).

https://doi.org/10.1016/j.sbsr.2024.100670
Received 17 March 2024; Received in revised form 19 June 2024; Accepted 24 June 2024
Available online 28 June 2024

chemical compounds and other analytes at very low concentrations. The high sensitivity and specificity of SPR sensors have led to their widespread use in biological and chemical sensing applications. One interesting development in SPR sensing technology is the integration of photonic crystal fibers (PCF). A unique class of optical fibers known as photonic crystal fibers (PCFs) are defined by a periodic arrangement of microcapillaries that surround a solid or hollow core of the fiber as its cladding [12]. Also, the microstructure of PCF, which provides exact control over light propagation, ensures single-mode operation and effective confinement of the light within the fiber core. There are numerous advantages to this unique design for SPR sensing applications. For example, this enables guided light to engage with the surroundings more successfully, enhancing sensing abilities [13]. Furthermore, by enabling the modification of parameters like pitch and air hole, PCF provides flexibility in the construction of sensors with adaptable sensitivity and response [14].

Cancer is characterized by uncontrolled cell proliferation, which is frequently caused by a single defective cell [15]. Cancer cells can infect nearby tissues, spread throughout the body, enter remote areas, and promote the formation of new blood vessels to feed them. This arises from the lack of the typical mechanisms that regulate the growth and dissemination of cancer cells. Cancerous (malignant) cells can arise from any tissue in the body. Cancer is currently one of the major causes of death. Approximately 10 million deaths in 2020 are attributed to cancer, according to the estimates of the World Health Organization. [16]. Some common forms of cancer in humans are blood cancer, skin cancer, cervical cancer, breast cancer, and adrenal gland cancer. Blood cancer, also known as hematologic cancer, refers to malignancies that originate in the blood, bone marrow, or lymphatic system [17]. Leukemia, lymphoma, and myeloma are the most common types of blood cancers. Adrenal gland cancer, on the other hand, is a rare and aggressive form of cancer that originates in the adrenal glands, which are responsible for producing hormones such as cortisol and adrenaline [18]. If not identified and treated promptly, breast cancer, which is one of the most common types of cancer in women, impacts the breast tissue and has the potential to spread to other areas of the body [19]. Skin cancer is a form of cancer that begins in the cells of the skin. It arises when specific skin cells undergo abnormal transformations, causing uncontrolled growth and division. Among the various types of skin cancer, Basal Cell Carcinoma (BCC) is the most prevalent [20] and typically originates in the basal cells found in the deepest layer of the epidermis, which is the outermost skin layer. Cervical cancer arises from the cells of the cervix. It is frequently linked to a persistent infection with high-risk types of the Human Papillomavirus (HPV) [21]. Early detection of these cancers plays a critical role in ensuring effective treatment and improved patient outcomes. Malignant cells are classified into stages I, II, and III, with stage I offering potential for cure, while stage III remains incurable [22]. Thus, early cancer cell detection becomes imperative for more successful treatment strategies. Although multiple blood tests, such as complete blood counts, blood protein analyses, tumor marker analyses, and urine examinations, are commonly conducted to detect cancer, they often fail to pinpoint the affected organ [23]. Biopsy, involving the examination of suspect cells, remains the most reliable method for identifying malignant cells [24]. Various diagnostic techniques, such as positron emission tomography (PET), ultrasound tests, magnetic resonance imaging (MRI), and computed tomography (CT) scans, are also utilized to locate tumors [25–27]. However, the time-consuming nature of these procedures, ranging from two minutes to several days, may adversely affect cancer patients who require prompt diagnosis. To address this, researchers in optoelectronics are striving to develop rapid cancer cell detectors. Due to the differences in refractive index (RI) between normal and malignant cells, they exhibit distinct light propagation behaviors when exposed to the same light source. Analyzing the received signal enables the determination of cell characteristics. Therefore, driven by a resolute desire to confront the enormous obstacles presented by cancer, this research work sets out to develop, construct, and deploy a Surface Plasmon Resonance-Photonic Crystal Fiber (SPR-PCF) biosensor for cancer identification with high sensitivity. The alarmingly high global cancer burden highlights the critical need for reliable, sensitive, and reasonably priced diagnostic technologies that can support early intervention and enhance patient outcomes. Surface Plasmon Resonance (SPR) and Photonic Crystal Fiber (PCF) integration offer a novel platform for the investigation of cutting-edge sensing methods, and it signifies a paradigm shift in biosensor design. SPR is used because of its extraordinary sensitivity and is well-known for its capacity to identify molecular interactions at the interface of a metal film [28]. In the meantime, PCF, with its flexible design, offers an adaptable medium for exceptionally accurate guiding light [29]. In order to develop a new biosensor design that exceeds the constraints of current diagnostic instruments, the research aim is to leverage the synergistic effects of these two state-of-the-art technologies.

SPR-PCF sensors are innovative devices that leverage the principles of surface plasmon resonance and photonic crystal fiber technology to detect and analyze biomolecular interactions [30]. SPR-based PCFs have shown excellent efficacy in a variety of applications in the fields of optical communication and biosensing [31,32]. When a photon beam interacts with the core of a Photonic Crystal Fiber (PCF), the electromagnetic field extends partially into the cladding region. This interaction excites the surface electrons of plasmonic materials as the evanescent field interacts with the plasmonic metal surface. The resonance phenomenon between the frequency of the evanescent field and the frequency of electron oscillation on the surface leads to the generation of a CL peak [33]. When in resonance, the real part of the refractive index of the core mode and the SPP mode match, resulting in the highest energy transfer between them. The observation of the analyte's RI variation results in a shift in the peak's position at the resonant wavelength. This opens the door for SPR-PCF sensors to detect a broad variety of analytes. So, It is now possible to achieve improved biosensing thanks to the efficiency of PCF-SPR sensors. The use of SPR-PCF sensors in cancer detection offers several advantages, including high sensitivity [34] and specificity, allowing for the detection of even minute concentrations of cancer-related biomarkers. Additionally, these sensors are non-invasive [35] or minimally invasive, providing a non-destructive and real-time monitoring platform. Researchers are now studying different designs for SPR-PCF biosensors for cancer detection thanks to recent technological advances in the field. An SPR-PCF biosensor was proposed by **Yasli A.** [36] to detect cancer early in life using a single living cell. Numerical analyses are performed using the Full vectorial Finite Element Method (FV-FEM) with perfectly matched layers. To find the refractive index (RI) variations of cancer cells, two techniques are used: spectral interrogation and amplitude. Six distinct cancerous cell types had refractive index (RIs) ranging from 1.38 to 1.401. The biosensor was able to measure the maximum Amplitude Sensitivity (AS) of $-757\ \text{RIU}^{-1}$ for HeLa cells and the maximum Wavelength Sensitivity (WS) of 7142.86 nm/RIU for Breast cancer Type-2 (MCF-7) cells. A double-core photonic crystal fiber (PCF) based refractive index sensor was introduced by **Ehyaee et al.** [37] to identify six distinct cancer-affected cell types. The fiber has a sizable central air hole that allows fluids containing both healthy and cancer-affected cells to be introduced. The suggested sensor in this work exhibits spectral sensitivities for basal cell cancer, cervical cancer (HeLa cells), Jurkat cancer cells, PC12 cancer cells, MDA-MB-231 breast cancer cells, and MCF-7 breast cancer cells of 10,000 nm/RIU, 11,250 nm/RIU, 10,714.28 nm/RIU, 12,857.14 nm/RIU, 11,428.57 nm/RIU, and 12,500 nm/RIU, respectively. Additionally, the investigation assesses resolution as a critical factor, producing 1×10^{-5} RIU, 8.89×10^{-6} RIU, 9.33×10^{-6} RIU, 7.78×10^{-6} RIU, 8.75×10^{-6} RIU and 8×10^{-6} RIU results for the aforementioned cells, in that order. **Mittal et al.** [34] presented an all-optical sensor architecture that uses a spiral-shaped photonic crystal fiber structure and the surface plasmon resonance effect to detect cancer cells. With a resolution of 2.33×10^{-4} RIU, the finite element method (FEM) simulations, which cover a variety of cancer cells including HeLa,

Basal, Jurkat, MDA-MB-231, MCF7, and PC12, show a maximum sensitivity of -289 RIU^{-1} for the detection of breast cancer cells. The refractive index range in which the sensor operates effectively is 1.36 to 1.401. A surface plasmon resonance (SPR) refractometric sensor based on gold (Au) and titanium dioxide (TiO_2) coated Photonic Crystal Fiber (PCF) was proposed by **Chaudhary et al.** [38] as a quick way to detect cancer cells. With an Au coating serving as the plasmonic material, the sensor operates on the surface plasmon resonance (SPR) principle and is intended for the rapid identification of a variety of cancerous cells, such as MDA-MB-231, MCF-7, PC-12, HeLa, and Jurkat, which correspond to breast cancer type-1, type-2, adrenal glands, cervical, and blood cancer, in that order. COMSOL Multiphysics software was utilized for the computational analysis, which yielded wavelength sensitivities ranging from 5500 nm/RIU to 10714.28 nm/RIU for various cancer cells. The maximum amplitude sensitivity varied between -1387 RIU^{-1} and -1599 RIU^{-1}. With a maximum detection limit of 0.024, the sensor resolution spans 0.93×10^{-5} RIU to 1.82×10^{-5} RIU. **Sardar et al.** [39] introduced a Dual Core Dual Polished PCF SPR Sensor designed for the detection of cancer cells, achieving the highest WS of 7143 nm/RIU for both breast Type-1 and Type-2 cancer cells. Additionally, it demonstrated the highest AS of -270 RIU^{-1} specifically for breast Type-1 cancer cells. **Abdelghaffar et al.** [40] introduced a dual V-shaped PCF biosensor with plasmonic technology designed specifically for the identification of cancer cells. For skin, cervical, and breast Type-1 cancer cells, their sensor showed significant WS of 23700 nm/RIU, 8208 nm/RIU, and 14428.6 nm/RIU, respectively. **Ibrahimi et al.** [41] put forth a sensitive Twin-Core PCF SPR biosensor with gold plating to accelerate cancer cell detection. The biosensor attained the highest WS of 4285.71 nm/RIU for breast type-1 and type-2 cancer cells, and AS of 4078.43 RIU^{-1} for cervical cancer cells. **Yang et al.** [42] developed a high-performance Photonic Crystal Fiber biosensor based on Surface Plasmon Resonance for rapid cancer detection, with a high WS of 16357 nm/RIU and AS of -1242 RIU^{-1} for breast type-2 cancer cells.

To enhance sensitivity and performance, a straightforward yet remarkably sensitive SPR-PCF biosensor using gold nanowires as plasmonic material which is tailored for the detection of cancer cells in the Adrenal gland, Blood, Breast (two cell types), Cervical, and Skin tissues is introduced. These six specific cell types are employed as analytes, and an extensive numerical investigation of the overall sensitivity is performed using the Finite Element Method (FEM). By employing a specially designed PCF geometry to analyze cancer cell samples, notable results are achieved with a substantial Wavelength Sensitivity (WS) of 35714.28 nm/RIU and an impressive Amplitude Sensitivity (AS) of -1971.30 RIU^{-1} for Breast Cancer Type-2 cells.

2. Structural design and numerical analysis

The complete intersection of the proposed SPR-PCF model is depicted in Fig. 1. A Physics-controlled mesh is employed providing a total of 147,037 degrees of freedom, with a fine element size to ensure maximum precision in the simulations. The overall structure consisted of 20,980 elements, characterized by a minimum element quality of 0.05026 and an average element quality of 0.8416. The element area ratio is 0.0001684, and the mesh area covers 415.1 μm^2. (See Fig. 2.)

The study utilized the Finite Element Method (FEM) as a computational tool to examine the properties of mode propagation [1]. The simulations were conducted using the COMSOL Multiphysics v5.5 program. The perfectly matched layer (PML) is utilized to absorb outgoing waves without reflecting any of them back into the bounded domain. Below the PML layer lies the unknown analyte layer, which is the target for detection. Silver (Ag) and gold (Au) are commonly employed as plasmonic materials within the photonic crystal fiber (PCF) structure [43]. However, the susceptibility of silver to oxidation in humid conditions poses a significant challenge [44], leading to a decrease in analyte detection accuracy. Consequently, gold emerges as the preferred metal of choice due to its stability, biocompatibility, and the substantial size of the resonance peak [45]. Gold (Au) nanowire is used as a plasmonic material because of its favorable plasmonic properties in the visible and near-infrared regions of the electromagnetic spectrum. Silica (SiO_2) is the fiber material employed in this design. The arrangement of air holes on a silica (SiO_2) substrate is designed to confine the electric field to the fiber's center and facilitate strong interaction with the Gold (Au) nanowire. Gold nanowires have a high surface area to volume ratio, allowing for more efficient binding of target molecules and improved sensitivity of the sensor [46]. The pitch distance, denoted as $\wedge$, corresponds to the separation between two adjacent cladding air holes. In the cladding, there are two different air hole diameters, namely D_1 and D_2. The air holes, characterized by a diameter D_1, are employed to confine light within the core region. The diminished size of air holes with diameter D_2 assists in lowering the CL by minimizing the scattering of light emanating from the fiber's center. The rectangular core's height and width are represented by H and W, respectively. The suggested

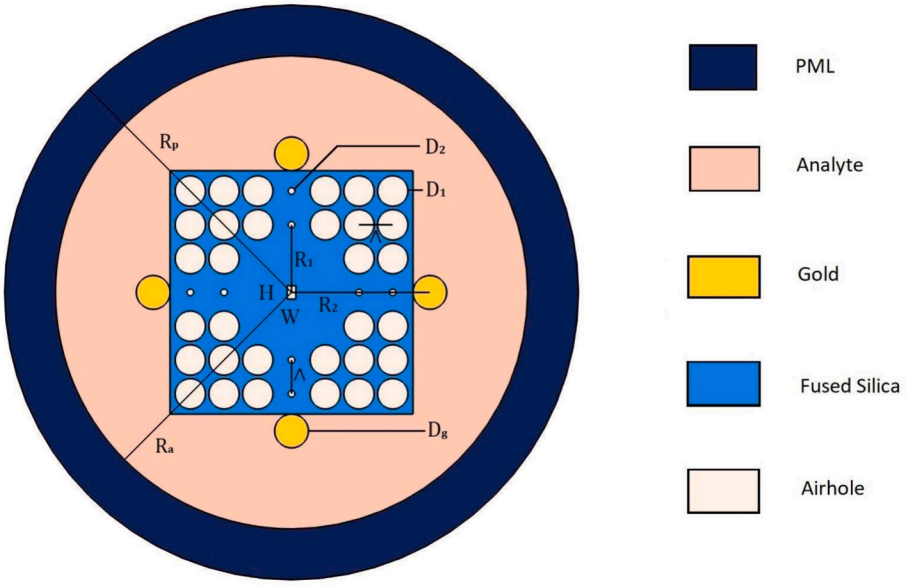

Fig. 1. Proposed design for the SPR-PCF structure.

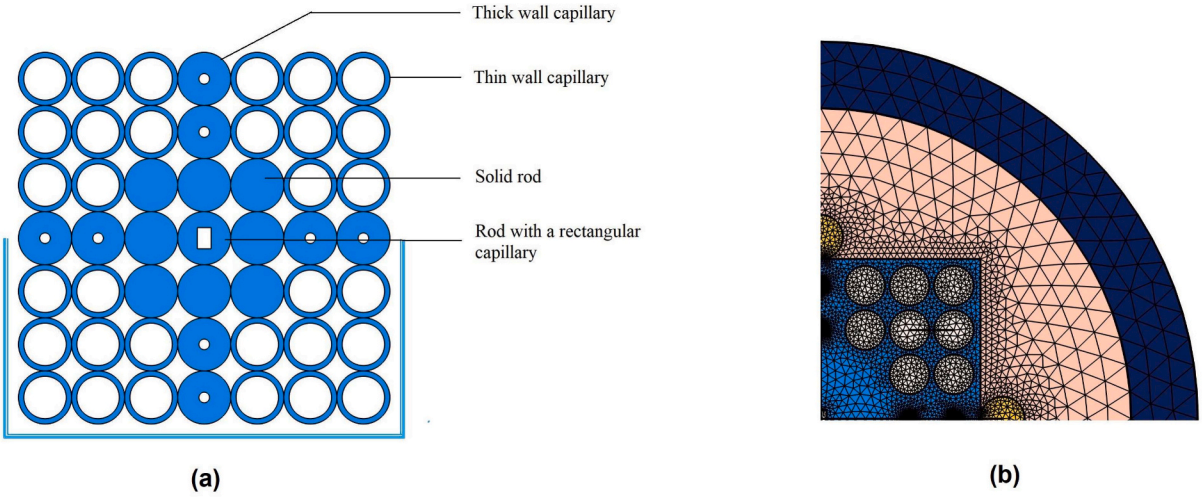

Fig. 2. Stacked preform and meshing output with boundary condition for the proposed SPR-PCF structure; (a) Stacked preform, (b) Meshing output (one-fourth of the PML layer computation window).

structural parameters for the PCF are as follows: $\wedge = 1\ \mu m$, $D_1 = 0.9\ \mu m$, μm, $D_2 = 0.2\ \mu m$, $R1 = 2\ \mu m$, $R2 = 4.1\ \mu m$, $W = 0.26\ \mu m$ and $H = 0.4\ \mu m$. Each side length of the square shaped cladding is $7.2\ \mu m$. The diameter of the gold nanowire is denoted by D_g. Optimum value for D_g is taken at $D_g = 1.0\ \mu m$. The diameter of the analyte and the perfectly matched layer (PML) are represented by $D_a = 2R_a = 20\ \mu m$ and $D_p = 2R_p = 23\ \mu m$.

The Finite Element Method (FEM) with a Perfectly Matched Layer (PML) boundary condition is widely used as a computational framework for numerically solving various problems. In our specific case, fused silica was used as the background material, and the refractive index of fused silica was determined using the Sellmeier equation, which can be expressed as follows: [47].

$$n^2(\lambda) = 1 + \frac{B_1\lambda^2}{\lambda^2 - C_1} - \frac{B_2\lambda^2}{\lambda^2 - C_2} - \frac{B_3\lambda^2}{\lambda^2 - C_3} \tag{1}$$

In this case, the refractive index of silica (n) is denoted, and the wavelength is measured in microns. The Sellmeier coefficients used to calculate the refractive index are as follows: $B_1 = 0.69616300$, $B_2 = 0.407942600$, $B_3 = 0.897479400$, $C_1 = 4.67914826 \times 10^{-3}\ \mu m^2$, $C_2 = 1.35120631 \times 10^{-2}\ \mu m^2$, and $C_3 = 97.9340025\ \mu m^2$.

In our proposed work, gold (Au) nanowires are employed. The dielectric constant of gold was determined using the Drude-Lorentz model [48], which is expressed by the following equation:

$$\varepsilon_{Au} = \varepsilon_\infty - \frac{\omega_D^2}{\omega(\omega + j\gamma_D)} - \frac{\Delta\varepsilon \cdot \Omega_L^2}{(\omega^2 - \Omega_L^2) + j\Gamma_L\omega} \tag{2}$$

The permittivity of the dielectric material (gold) is represented as ε_{Au}, while ε_∞ denotes its permittivity at high frequency with a value of 5.9673. The angular frequency, ω, can be defined as $\omega = 2\pi c/\lambda$, where c is the velocity of light in vacuum. Furthermore, the plasma frequency and damping frequency are denoted as ω_D and γ_D respectively, where $\omega_D/2\pi = 2113.6$THz and $\gamma_D/2\pi = 15.92$THz. The weighting factor is expressed as $\Delta\varepsilon = 1.09$. Furthermore, the Lorentz oscillators have a spectral width denoted as $\Gamma_L/2\pi = 104.86$THz and an oscillator strength denoted as $\Omega_L/2\pi = 650.07$THz.

The investigation of the proposed biosensor relies on a crucial parameter known as confinement loss (CL). The measurement of CL is conducted using the following Eq. [47]:

$$\alpha = 8.686 \times k_0 \times Im[n_{eff}] \times 10^4\ \text{dB/cm} \tag{3}$$

where $k_0 = 2\pi/\lambda =$ the number of free space, $\lambda =$ operating wavelength and $Im[n_{eff}] =$ the imaginary part of the effective refractive index.

3. Structural parameter optimization

In order to achieve optimum parameter values, the sensor performance is evaluated for various values, while keeping the remaining parameters constant. These outcomes pertain to the breast type-2 (MCF-7) cell detection process.

The following value for $D_1 = 0.9\ \mu m$, $D_2 = 0.2\ \mu m$, $W = 0.26\ \mu m$, and $H = 0.4\ \mu m$, $D_a = 20\ \mu m$ and $D_p = 23\ \mu m$ is taken to get optimum value for D_g and then at optimum D_g, other parameters are varied to get their optimum value. X-polarization values are taken to get the optimal value for parameters.

Starting with gold (Au) nanowire, the value for D_g is varied to $0.9\ \mu m$, $1.0\ \mu m$ and $1.1\ \mu m$ respectively. Comparing $0.9\ \mu m$ and $1.0\ \mu m$ gold diameter, it can be seen that the obtained CL for $0.9\ \mu m$ is less than $1.0\ \mu m$ in Fig. 3a. But the obtained AS for $0.9\ \mu m$ is $-1705.15\ \text{RIU}^{-1}$ and for $1.0\ \mu m$ is $-1971.30\ \text{RIU}^{-1}$ as shown in Fig. 3b. So $D_g = 1.0\ \mu m$ has higher AS. Also, the loss peak for normal and cancerous breast type-2 cell is at 1060 *nm* and 1470 *nm* respectively for $0.9\ \mu m$ D_g and 1040 *nm* and 1540 *nm* respectively for $1.0\ \mu m$ D_g. So the difference in wavelength shift between loss peaks for normal and cancerous breast type-2 cells increases from 410 *nm* to 500 *nm* when D_g is varied from $0.9\ \mu m$ to $1.0\ \mu m$ which results in WS increasing from 29285 nm/RIU to 35714.28 nm/RIU. So $1\ \mu m$ is better than $0.9\ \mu m$ for D_g. Now increasing this parameter value from $1.0\ \mu m$ to $1.1\ \mu m$, the sensor performance loses stability because the confinement loss increases too much and the leakage light in core mode is very high and no longer confined in the core for the analysis for RI at breast type-2 cancer cell. So, $1.0\ \mu m$ is chosen as the optimal value for D_g.

Airhole-1's diameter, D_1, is changed to $0.80\ \mu m$, $0.90\ \mu m$, and $1.0\ \mu m$, in that order. As can be seen in Fig. 4b, after comparing D_1 values for $0.80\ \mu m$ and $0.90\ \mu m$, the corresponding AS for $0.80\ \mu m$ is $-1758.63\ \text{RIU}^{-1}$, and for $0.90\ \mu m$ is $-1971.30\ \text{RIU}^{-1}$. This clearly shows the superiority of the latter. The loss peak for normal and cancerous breast type-2 cells are observed at 1010 *nm* and 1500 *nm*, respectively, for D_1 of $0.80\ \mu m$, and at 1040 *nm* and 1540 *nm*, respectively, for D_1 of $0.90\ \mu m$, as shown in Fig. 4a. The shift in wavelength between the loss peaks for normal and cancerous breast type-2 cells increases from 490 *nm* to 500 *nm* when D_1 is increased from $0.80\ \mu m$ to $0.90\ \mu m$, resulting in a WS increase from 35000 nm/RIU to 35714.28 nm/RIU. Consequently, D_1 of $0.90\ \mu m$ exhibits superior performance compared to $0.80\ \mu m$. However, when increasing this parameter to $1.0\ \mu m$, the sensor's performance becomes unstable due to a significant increase in confinement loss and excessive leakage of light in the core mode, no longer confined within

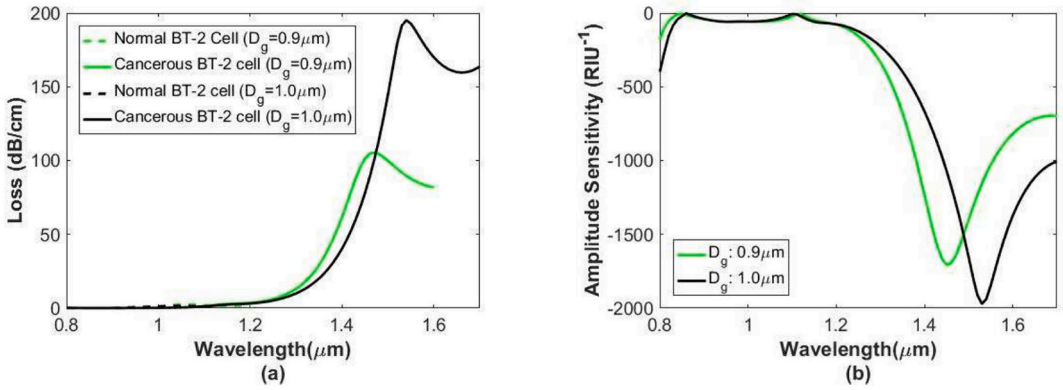

Fig. 3. Comparison between different gold diameters (D_g); (a) Confinement loss (b) Amplitude Sensitivity. (For interpretation of the references to color in this figure legend, the reader is referred to the web version of this article.)

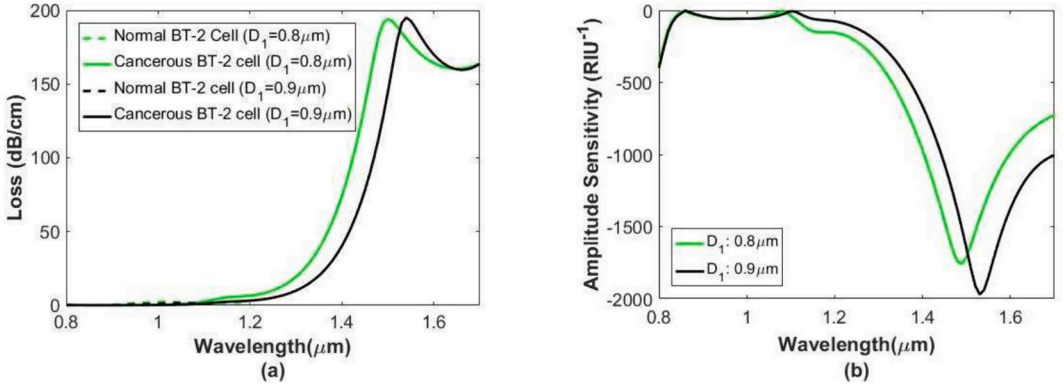

Fig. 4. Comparison between different Airhole-1 diameters (D_1); (a) Confinement loss (b) Amplitude Sensitivity.

the core during the analysis of RI at breast type-2 cancer cells. Therefore, 0.90 μm is designated as the optimal value for D_1.

Diameter of Airhole-2 (D_2) is varied to values of 0.40 μm, 0.20 μm, and 0.10 μm, respectively. Comparing D_2 values for 0.40 μm and 0.20 μm, the corresponding Amplitude Sensitivity (AS) for 0.40 μm is -973.39 RIU^{-1}, and for 0.20 μm is -1971.30 RIU^{-1}, as depicted in Fig. 5b, clearly establishing the latter's superiority. Loss peak for normal and cancerous breast type-2 cells are noted at 1050 nm and 1370 nm, respectively, for D_2 of 0.40 μm, and at 1040 nm and 1540 nm, respectively, for D_2 of 0.20 μm, as illustrated in Fig. 5a. The shift in wavelength between the loss peaks for normal and cancerous breast type-2 cells increases from 320 nm to 500 nm when D_2 is reduced from 0.40 μm to 0.20 μm, resulting in a WS increase from 22857.14 nm/RIU to 35714.28 nm/RIU. As a result, a diameter of D_2 at 0.20 μm exhibits superior performance when compared to 0.40 μm. However, diminishing this parameter further to 0.10 μm leads to an unstable performance of the proposed sensor, attributed to a significant rise in confinement loss and excessive leakage of light in the core mode. This light is no longer confined within the core during the analysis of the Refractive Index (RI) in breast type-2 cancer cells. So, 0.20 μm is identified as the optimal value for D_2.

For the analyte layer, the sensor is analyzed with three different values of D_a respectively 16 μm, 20 μm and 24 μm. Comparing D_a values for 16 μm and 20 μm, the corresponding AS for 16 μm is -1716.44 RIU^{-1}, and for 20 μm is -1971.30 RIU^{-1}, as depicted in Fig. 6b, clearly establishing the latter's superiority. But the WS is same for both values

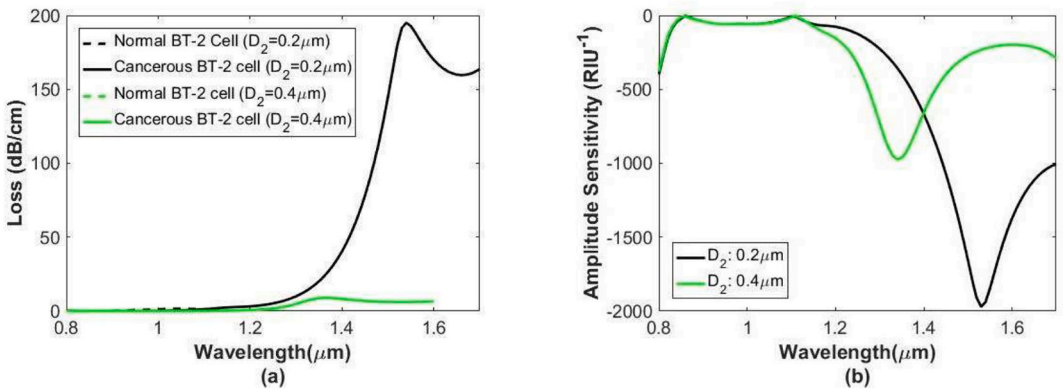

Fig. 5. Comparison between different Airhole-2 diameters (D_2); (a) Confinement loss (b) Amplitude Sensitivity.

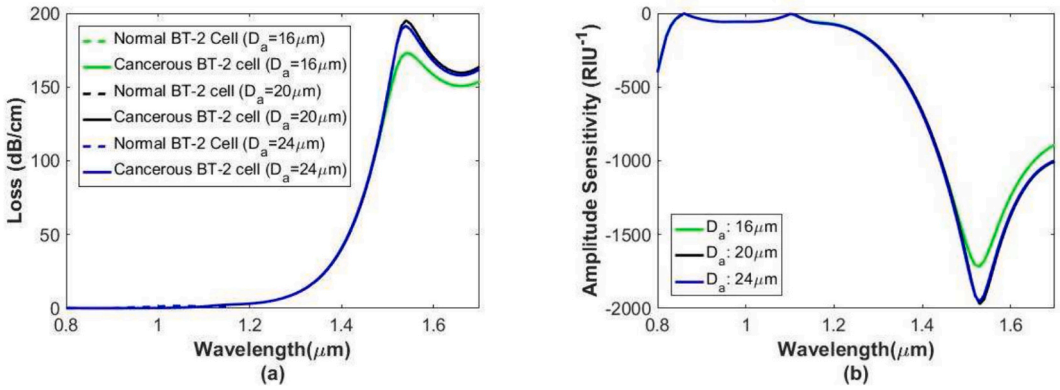

Fig. 6. Comparison between different analyte layer diameters (D_a); (a) Confinement loss (b) Amplitude Sensitivity.

since the loss peak for normal and cancerous breast type-2 cells are noted at 1040 *nm* and 1540 *nm*, respectively in both cases, as illustrated in Fig. 6a. Now if D_a is increased to 24 μm, it can be seen that the value of AS is -1955.62 RIU^{-1} which is less than the AS obtained for $D_a = 20$ μm. Also, the WS remains the same for all three values. Hence, $D_a = 20$ μm is taken as the optimal value.

The size of the rectangular hollow core is varied while maintaining a consistent ratio between W and H. The dimensions explored are: $W = 130$ *nm* and $H = 200$ *nm*, $W = 260$ *nm* and $H = 400$ *nm*, and $W = 390$ *nm* and $H = 600$ *nm*, respectively. This variation is evident in Fig. 7b. Upon comparing the first two size variations ($W = 130$ *nm* and $H = 200$ *nm*, $W = 260$ *nm* and $H = 400$ *nm*), the corresponding AS for the first core size is -761.36 RIU^{-1}, while for the second core size, it is -1971.30 RIU^{-1}. This clearly shows that the latter is better. For the first core size ($W = 130$ *nm* and $H = 200$ *nm*), the loss peaks for normal and cancerous breast type-2 cells are observed at 980 *nm* and 1300 *nm*. On the other hand, for the second core size ($W = 260$ *nm* and $H = 400$ *nm*), the loss peaks are found at 1040 *nm* and 1540 *nm*, as depicted in Fig. 7a. The shift in wavelength between the loss peaks for normal and cancerous breast type-2 cells increases from 320 *nm* to 500 *nm* when transitioning from the first core size to the second core size, resulting in a WS increase from 22857.14 nm/RIU to 35714.28 nm/RIU. So, the second core size exhibits superior performance compared to the first one. Nevertheless, the performance of the sensor becomes unstable when taking into account the third core size variation ($W = 390$ *nm* and $H = 600$ *nm*) because of a notable rise in confinement loss and excessive light leakage in the core mode, which is no longer confined within the core during the analysis of refractive index at breast type-2 cells. This instability results in the inability to identify a confinement loss peak in normal breast type-2 cells and the failure of the resonance condition to be met in cancerous breast type-2 cells. Consequently, it is determined that the ideal value for the rectangular hollow core size is $W = 260$ *nm* and $H = 400$ *nm*.

A Perfectly Matched Layer (PML) in Surface Plasmon Resonance (SPR) Photonic Crystal Fiber (PCF) sensors is typically used to minimize reflection and effectively absorb outgoing waves at the boundary of the computational domain [49]. It's not a physical layer that exists in practical sensor implementations or real-world applications. so the thickness of pml is taken about 15% of total sensor size which can be obtained if $D_p = 23$ μm. But PML is still varied D_p to 22 μm and 24 μm from 23 μm to observe if any change occurs but almost the same result was observed for AS and WS for those values as seen in Fig. 8a and Fig. 8b. so 23 μm was retained as the value for D_p.

It is to be noted that the proposed SPR-PCF sensor is designed and optimized for x-polarization values to get maximum sensitivity. So, further investigations will be done using x-polarization values. Polarizer controller is used to control the polarization state [50] in the experimental setup.

4. Simulation results and discussions

Fig. 9 shows the core and SPP modes for our proposed biosensor design. Fig. 10 shows the phase matching of the blood (normal) cells. The resonance condition of the blood (normal) cells depicted in Fig. 10 is demonstrated as follows: the effective index of the fundamental (core-mode) (green-dotted line) and plasmon modes (SPP-mode) (blue-dotted line) intersect at a wavelength of 880 *nm*. At this specific wavelength, there is a notable high-energy transformation from the fundamental mode to the plasmon mode, resulting in the propagation losses reaching their maximum values. This observation is indicative of the resonance condition.

Wavelength sensitivity (WS) refers to the change in the resonance wavelength of the SPR sensor in response to changes in the refractive

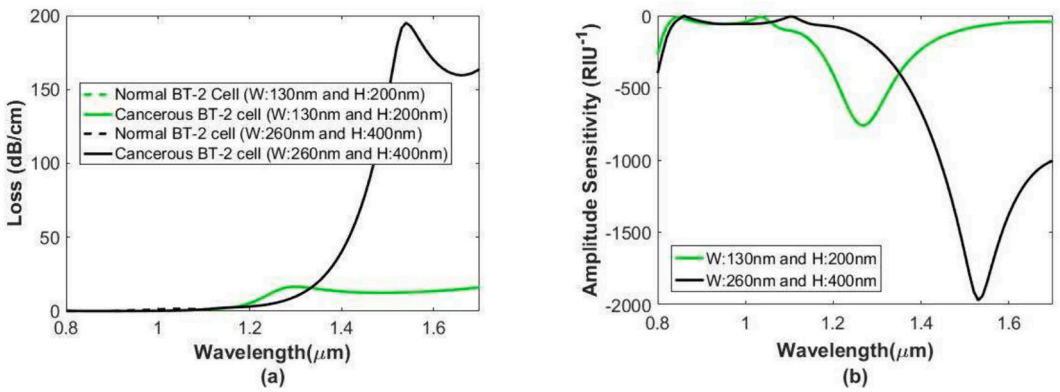

Fig. 7. Comparison between different rectangular hollow core sizes; (a) Confinement loss (b) Amplitude Sensitivity.

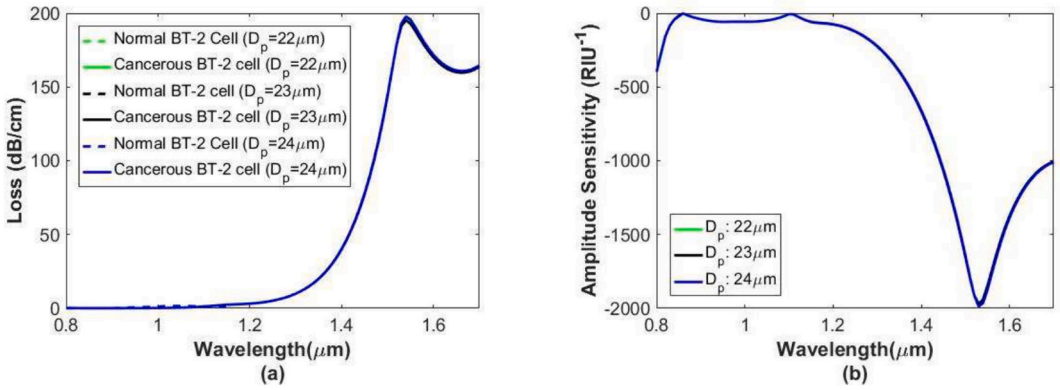

Fig. 8. Comparison between different pml diameters (D_p); (a) Confinement loss (b) Amplitude Sensitivity.

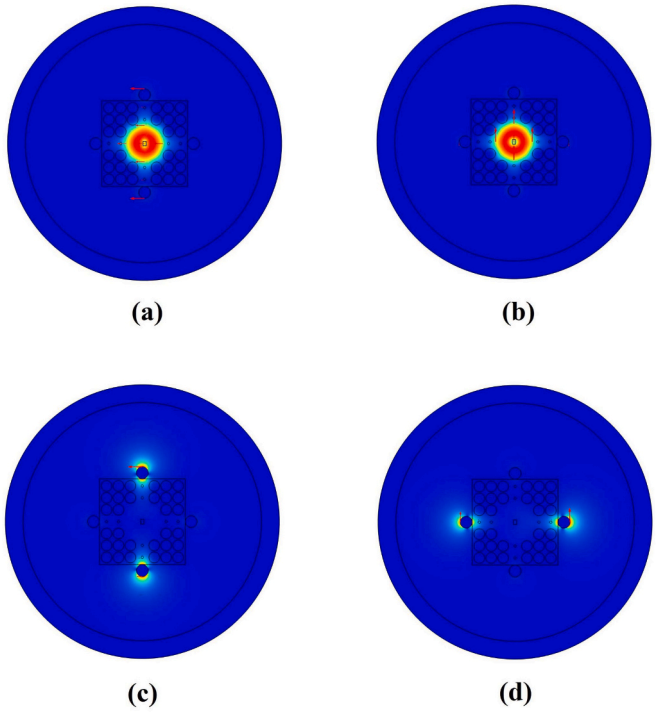

Fig. 9. Electric field distribution for the proposed sensor; (a) Core mode x-axis (E_x), (b) Core mode y-axis (E_y), (c) SPP mode x-axis (E_x) and (d) SPP mode y-axis (E_y).

index of the medium in contact with the sensor surface [51]. When the refractive index of the medium in contact with the sensor surface changes, the resonance condition for SPR is altered, leading to a shift in the wavelength at which maximum SPR occurs. Wavelength sensitivity is often expressed in terms of the change in resonance wavelength per unit change in refractive index (typically in nanometers per refractive index unit, nm/RIU). Confinement loss (CL) in photonic crystal fiber (PCF) refers to the loss of light that occurs due to the confinement of the optical mode within the photonic crystal structure of the fiber [52]. This parameter is very important for calculating WS of our SPR-PCF sensor. Because the confinement loss curve has a peak value when the SPR occurs. Confinement loss curve for different normal and cancer cells are given in Fig. 11. WS is calculated using the following Eq. [53]:

$$S_\lambda = \frac{\Delta\lambda_{\text{peak}}}{\Delta n_a}\ \text{nm}\Big/\text{RIU} \tag{4}$$

where the term $\Delta\lambda_{\text{peak}}$ represents the variance between the wavelengths

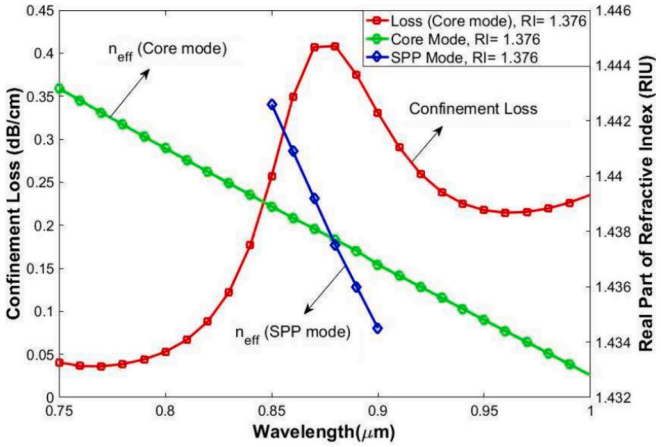

Fig. 10. Phase matching of core and SPP mode.

of two neighboring peak losses, while Δn_a signifies the difference between the corresponding refractive index.

Amplitude sensitivity (AS), on the other hand, refers to the change in the amplitude of the SPR response curve in response to changes in the refractive index of the medium. The amplitude of the SPR curve corresponds to the intensity of the reflected light at the resonance condition. Changes in the refractive index of the medium affect the width and shape of the SPR curve, resulting in variations in the amplitude. Amplitude sensitivity is often expressed as the change in reflectivity or intensity per unit change in refractive index. The following equation is used to measure AS [53]:

$$S_A(\lambda) = -\frac{1}{a(\lambda, n_a)}\frac{\partial a(\lambda, n_a)}{\partial n_a}\text{RIU}^{-1} \tag{5}$$

here, $a(\lambda, n_a)$ refers to the total propagation loss at a particular refractive index (RI) equal to n_a, while $\partial a(\lambda, n_a)$ represents the disparity between the two loss spectra.

Fig. 12 displays the relationship between AS and wavelength for six distinct types of cancer cells: Skin Cancer, Cervical Cancer, Blood Cancer, Adrenal Gland Cancer, Breast Cancer Type-1, and Breast Cancer Type-2. Upon analyzing the figure, it becomes apparent that Breast Cancer Type-2 exhibits the highest AS of $-1971.31\ \text{RIU}^{-1}$ compared to the other cancer cell types. A negative value for amplitude sensitivity indicates a decrease in the amplitude of the SPR response curve with respect to changes in the refractive index of the surrounding medium. In practical terms, this means that as the refractive index increases, the amplitude of the reflected light signal associated with SPR decreases. The amplitude of the SPR curve is often associated with the intensity of the reflected light. Therefore, a negative amplitude sensitivity implies a

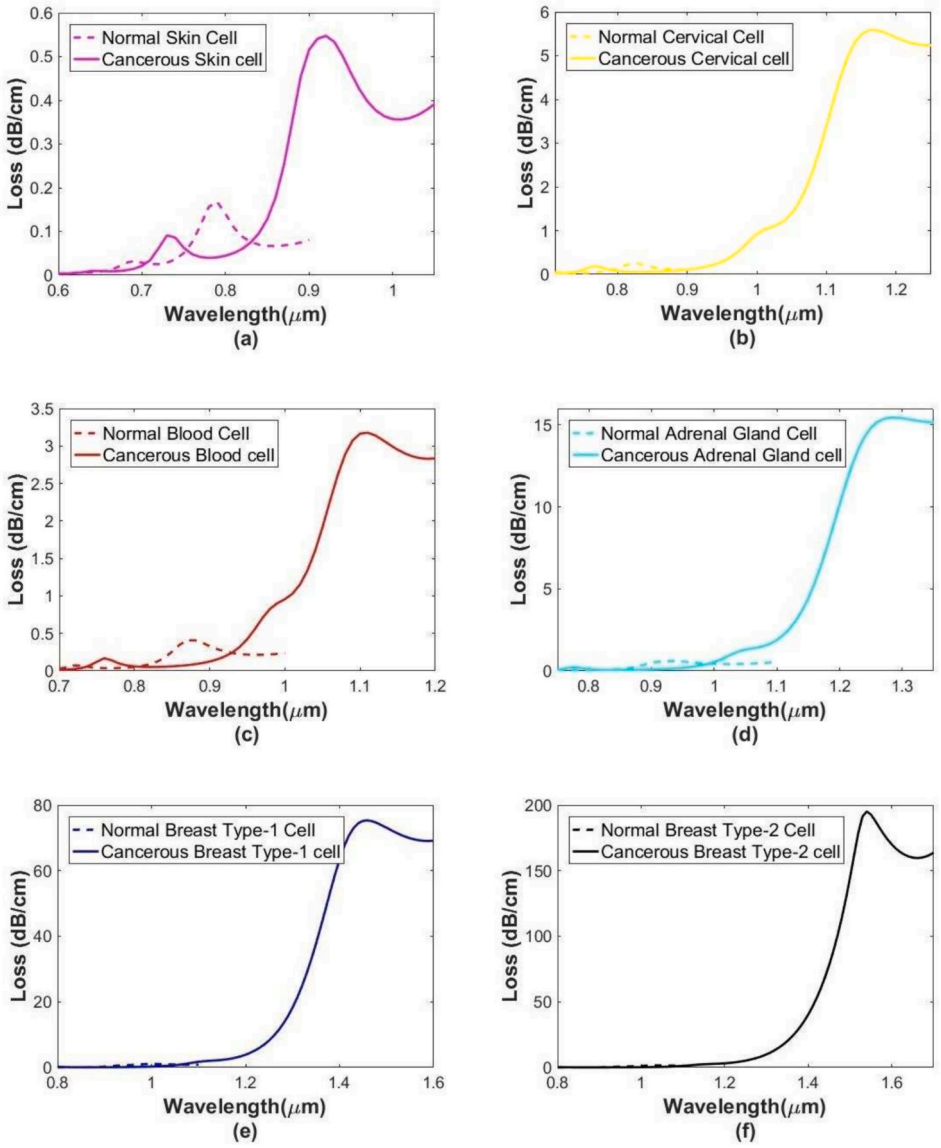

Fig. 11. Confinement loss curve for different normal and cancerous cells; (a) Skin, (b) Cervical, (c) Blood, and (d) Adrenal Gland, (e) Breast Type-1 and (f) Breast Type-2.

reduction in signal intensity as the conditions for SPR are modified.

Small variations in RI measurement can be accurately discerned and faithfully portrayed only when the sensor possesses a sufficiently high resolution. This parameter is calculated for both the amplitude and wavelength investigation methods through the application of Eqs. (6) and (7), respectively, as referenced in [53].

$$R_A = \frac{\Delta n_A}{S_A}(\text{RIU}), \tag{6}$$

$$R(w) = \frac{\Delta \lambda_{\min}}{S_\lambda}(\text{RIU}), \tag{7}$$

Here, Δn_A represents the interval between two successive refractive index, S_A denotes the amplitude sensitivity, $\Delta\lambda_{\min} = 0.1nm$ signifies the minimum wavelength resolution, and S_λ indicates the wavelength sensitivity. The proposed sensor exhibits a resolution of 7.10×10^{-6} RIU for Breast Type-2 cancer cell detection determined by Eq. (6). Additionally, the sensor achieves a resolution of 2.80×10^{-6} RIU for the same cancer cell detection using Eq. (7). Thus, the sensor demonstrates the capability to detect subtle refractive index variations on the order of 10^{-6}.

Table 1 represents the associated WS and AS values for the proposed SPR-PCF biosensor across six different cancer cell types, including Skin, Cervical, Blood, Adrenal gland, Breast Type-1, and Breast Type-2 cells. It also shows the resolution(wavelength) and resolution(amplitude) for the aforementioned cancer cells. Notably, Breast Cancer Type-2 demonstrates the highest WS of 35714.28 nm/RIU, as evidenced by the data in the table. Table 2 shows the comparison in sensitivity between the proposed SPR-PCF biosensor and previous cancer detection sensors. Some recent PCF sensors exhibit very high sensitivity within their maximum RI range [54–57]. However, within the similar range where our proposed sensor demonstrates the highest wavelength and amplitude sensitivity, which is for Breast Type-2 cancer cells (RI range 1.387–1.401), these sensors show lower sensitivity compared to our proposed sensor.

The linearity response is a crucial parameter in sensor design [36], as it determines the performance of the sensor for various applications. A high linearity response is desirable. Fig. 13 illustrates the linear fitting graph depicting the relationship between resonance wavelengths. The linearity of the proposed SPR-PCF sensor was evaluated using MATLAB curve fitting, where the slope of the linear fitting curve was measured

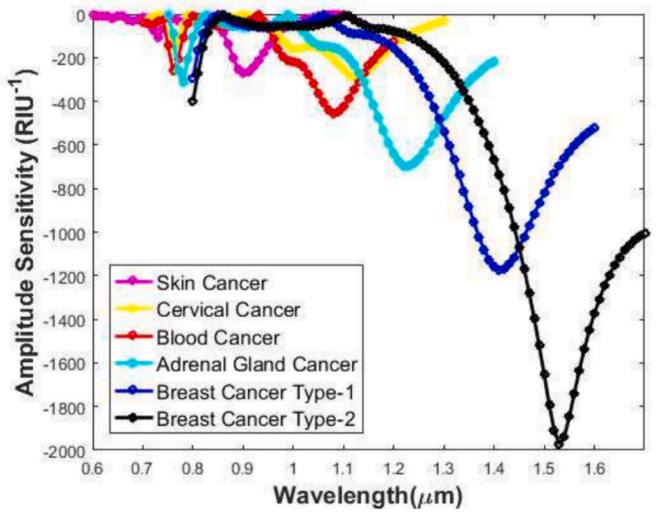

Fig. 12. Amplitude Sensitivity for different cancer cells.

with respect to the resonance angle. If the sensor exhibits linearity, it becomes easier to predict the resonance angle for higher analyte refractive indices. Conversely, sensor nonlinearity introduces significant variability and complicates the detection process. Consequently, nonlinearity is an undesirable characteristic in a sensor. The linearity is quantified using the correlation coefficient (R), obtained through linear regression analysis. For the proposed sensor, the regression equation for the linear fit is $y = 29870x - 40356$, with a regression coefficient of $R^2 = 0.9534$, as illustrated in Fig. 13. The correlation coefficient's value, close to 1, demonstrates a high degree of linearity, approaching the ideal condition.

5. Fabrication of the proposed SPR-PCF biosensor

Upon achieving superior performance, the implementation of the biosensor for cancer cell detection becomes highly advantageous. Consequently, the aim is to delve into the fabrication possibilities of our proposed design. Fabrication holds significant importance in microstructured fibers, given their numerous intricately shaped minuscule holes. Fortunately, the relentless advancement of technologies ensures the feasibility of fabricating structures encompassing a diverse array of shapes. Various manufacturing methodologies, including boiling techniques, capillary packing, multiple thinning, casting, sol-gel, stacking, and the drawing method [61–69], have been employed to generate hollow-shaped processes. Notably, 3D printing has been leveraged to craft numerous hollow-shaped core processes [69]. D. Pysz et al. have successfully employed the stack and draw technique to produce several photonic crystal fiber (PCF) structures [68]. Furthermore, Z. Lui et al. [66] have presented diverse stack and draw techniques specifically tailored for fabricating suspended microstructure fibers. The stack-and-draw method is recommended for fabricating the proposed sensor, as this method has been suggested for the fabrication of many similar types of sensors. [5,53,70].

The proposed sensor's gold nanowire diameter (D_g), large airhole diameter (D_1), and small airhole diameter (D_2) may not precisely match the optimal values. Existing routine procedures typically exhibit a variance of ±1% or ± 2% in proportions [53]. To evaluate the sensor's adaptability, a fabrication tolerance study is conducted. Fig. 14 and Table 3 demonstrate that variations in air hole diameter by ±1%, ±2% and ± 3% have minimal impact on the sensor's CL. The sensor's CL increases slightly when the diameter of the two air holes is reduced and decreases when the diameter is increased. The peak wavelength is also almost the same up to ±3% change in both air hole diameters. So, the sensor remains highly adaptable, showing insignificant changes even with a ± 3% variation in dimensions. However, fluctuations in the diameter of gold nanowires cause more noticeable changes in CL compared to variations in air hole sizes. So, precise construction of the gold nanowire is crucial for achieving nearly accurate values.

6. Conclusions

To sum up, this paper presents a highly sensitive biosensor for classifying and identifying different types of cancer cells. The proposed Surface Plasmon Resonance Photonic Crystal Fiber (SPR-PCF) biosensor, which uses gold nanowires as the plasmonic material, is a promising biosensor that exhibits remarkable sensitivity against six different types of cancer cells: adrenal gland cancer, blood cancer, breast type-1 cancer, breast type-2 cancer, cervical cancer and skin cancer. With its enhanced design the biosensor performs better overall, both in terms of sensitivity and efficiency. The biosensor's WS peaks at 35714.28 nm/RIU and AS peaks at −1971.30 RIU^{-1} for Breast type-2 cancer cells. The improved performance of our proposed biosensor in cancer cell detection is further validated by comparing it with previous PCF structures in Table 2.

There are some restrictions to be aware of with our study. To achieve high sensitivity, surpassing standard shapes was necessary, and a slightly complex model, which may be moderately difficult to fabricate, had to be created. Nevertheless, a likely method for fabrication is suggested for the proposed SPR-PCF biosensor. It's also critical to remember that the performance of the proposed biosensor could be impacted by environmental elements like pH, humidity, and temperature.

In spite of its minor drawbacks, the proposed biosensor holds great promise for integrating additional bioapplications, like 3D-Printed Microneedles (MNs) [71] and Microfluidic Invasion Chemotaxis Platform for 3D Neurovascular Co-Culture [72], to enhance overall functionality and enhance user experience. The Microfluidic Invasion Chemotaxis Platform for 3D Neurovascular Co-Culture can be used to simulate human diseases and study tissue and organ models in order to evaluate our biosensor's performance for detection in multicellular systems. In addition, since 3D-Printed MNs are easy to use and less

Table 1
The optical properties of the proposed SPR-PCF biosensor for cancer detection.

Cancer Type	Cell Type	State [58]	RI	WS (nm/RIU)	AS (RIU^{-1})	Res. (Wl) (RIU)	Res. (Amp) (RIU)
Skin	Basal	Normal (30–70%) Cancerous (80%)	1.36 1.38	6500	−273.16	1.54×10^{-5}	7.32×10^{-5}
Cervical	HeLa	Normal (30–70%) Cancerous (80%)	1.368 1.392	14,583.33	−286.58	6.86×10^{-6}	8.37×10^{-5}
Blood	Jurkat	Normal (30–70%) Cancerous (80%)	1.376 1.39	16,428.57	−455.59	6.09×10^{-6}	3.07×10^{-5}
Adrenal Gland	PC-12	Normal (30–70%) Cancerous (80%)	1.381 1.395	25,714.28	−698.76	3.89×10^{-6}	2.00×10^{-5}
Breast Type-1	MDA -MB -231	Normal (30–70%) Cancerous (80%)	1.385 1.399	32,857.14	−1172.72	3.04×10^{-6}	1.19×10^{-5}
Breast Type-2	MCF-7	Normal (30–70%) Cancerous (80%)	1.387 1.401	35,714.28	−1971.30	2.80×10^{-6}	7.10×10^{-6}

Table 2
The optical properties comparison of the proposed SPR-PCF biosensor with previous sensors for cancer detection (Red color indicates the highest sensitivity achieved for that specific sensor).

Ref	Sensor Type	Cancer Cell	WS (nm/RIU)	AS (RIU^{-1})
[36]	SPR-PCF	Adrenal Gland (PC-12)	5500	−399
		Blood (Jurkat)	4642.86	−401
		Breast Type-1 (MDA-MB-231)	6428.57	−324
		Breast Type-2 (MCF-7)	7142.86	−305
		Cervical (HeLa)	4333.33	−757
		Skin (Basal)	3150	−625
[34]	SPR-PCF	Adrenal Gland (PC-12)	–	−245.5
		Blood (Jurkat)	–	−165.9
		Breast Type-1 (MDA-MB-231)	–	−289
		Breast Type-2 (MCF-7)	–	−154.5
		Cervical (HeLa)	–	−166.7
		Skin (Basal)	–	−83
[37]	dual-core PCF	Adrenal Gland (PC-12)	12,857.14	–
		Blood (Jurkat)	10,714.28	–
		Breast Type-1 (MDA-MB-231)	11,428.57	–
		Breast Type-2 (MCF-7)	12,500	–
		Cervical (HeLa)	11,250	–
		Skin (Basal)	10,000	–
[38]	SPR-PCF	Adrenal Gland (PC-12)	7571.43	−1452
		Blood (Jurkat)	6000	−1599
		Breast Type-1 (MDA-MB-231)	9428.57	−1441
		Breast Type-2 (MCF-7)	10,714.28	−1411
		Cervical (HeLa)	5500	−1387
[39]	PCF-SPR	Adrenal Gland (PC-12)	6429	−259
		Blood (Jurkat)	5714	−203
		Breast Type-1 (MDA-MB-231)	7143	−270
		Breast Type-2 (MCF-7)	7143	−249
		Cervical (HeLa)	5000	−221
		Skin (Basal)	3500	−152.
[40]	Dual V-shaped SPR-PCF	Breast Type-1 (MDA-MB-231)	14,428.6	–
		Cervical (HeLa)	8208	–
		Skin (Basal)	23,700	–
[41]	Twin-Core PCF-SPR	Adrenal Gland (PC-12)	3571.42	−2537.37
		Blood (Jurkat)	3571.42	−2172.31
		Breast Type-1 (MDA-MB-231)	4285.71	−2193.76
		Breast Type-2 (MCF-7)	4285.71	−1813.13
		Cervical (HeLa)	2916.66	−4078.43
		Skin (Basal)	2500	−1611.02
[42]	SPR-PCF	Adrenal Gland (PC-12)	12,000	−902
		Blood (Jurkat)	9786	−713
		Breast Type-1 (MDA-MB-231)	14,500	−1108
		Breast Type-2 (MCF-7)	16,357	−1242
		Cervical (HeLa)	9000	−557
		Skin (Basal)	6450	−371
[59]	H-Shaped SPR-PCF	Breast Type-1 (MDA-MB-231)	7857.14	−985.27
		Cervical (HeLa)	5000	−792.89
		Skin (Basal)	4000	−422.76
[60]	D-shaped SPR-PCF	Adrenal Gland (PC-12)	17,857.14	–
		Blood (Jurkat)	23,214.28	–
		Breast Type-1 (MDA-MB-231)	19,285.71	–
		Breast Type-2 (MCF-7)	22,857.14	–
		Cervical (HeLa)	17,916.66	–
		Skin (Basal)	18,000	–
Proposed Sensor	SPR-PCF	Adrenal Gland (PC-12)	25,714.28	−698.76
		Blood (Jurkat)	16,428.57	−455.59
		Breast Type-1 (MDA-MB-231)	32,857.14	−1172.72
		Breast Type-2 (MCF-7)	35,714.28	−1971.30
		Cervical (HeLa)	14,583.33	−286.58
		Skin (Basal)	6500	−273.16

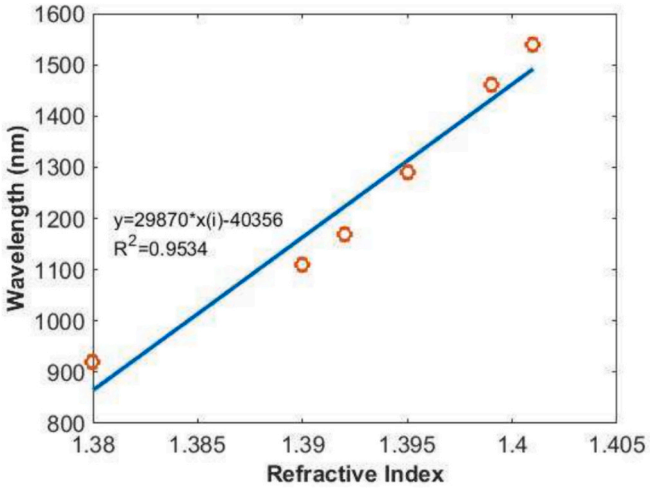

Fig. 13. Linear fitting characteristics of the proposed biosensor.

invasive than conventional needles, they can be used to collect analytes from the human body for our proposed sensor with less discomfort and tissue damage. The authors express a strong belief in the considerable potential of the proposed SPR-PCF biosensor for highly sensitive cancer cell detection. With the help of new developments in nanofabrication technologies, it is expected that this biosensor can be produced using the suggested fabrication method or other approaches.

Author statement

We declare that this manuscript is original, has not been published before and is not currently being considered for publication elsewhere.

We confirm that the manuscript has been read and approved by all named authors and that there are no other persons who satisfied the criteria for authorship but are not listed.

We further confirm that the order of authors listed in the manuscript has been approved by all of us.

We understand that the Corresponding Author is the sole contact for the Editorial process. He is responsible for communicating with the other authors about progress, submissions of revisions and final approval of proofs.

Stated by all authors as follows:

1. Atiqul Alam Chowdhury (First Author)
2. Md Rezaul Hoque Khan (Corresponding Author)

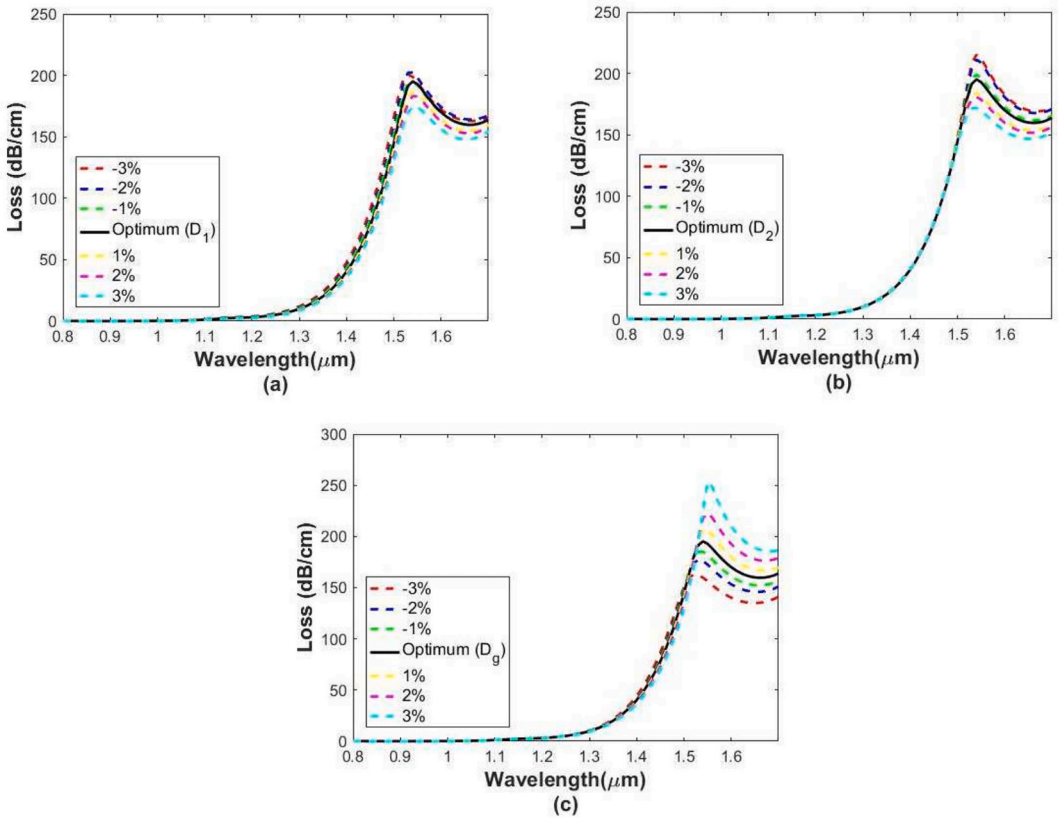

Fig. 14. CL curve at Breast Type-2 cancer cell (RI = 1.401), showing ±1%, ±2% and ± 3% variation in D_1, D_2 and D_g; (a) variation in D_1, (b) variation in D_2 and (c) variation in D_g.

Table 3
Consequence of varying the air hole and gold nanowire diameter on the CL of the sensor.

Change in Dimension	Variation in D_1, CL peak (dB/cm)	Variation in D_2, CL peak (dB/cm)	Variation in D_g, CL peak (dB/cm)
−3%	200.87	215.13	162.90
−2%	202.29	211.19	177.21
−1%	195.19	199.09	185.19
0%	195.13	195.13	195.13
1%	186.40	183.87	207.15
2%	183.19	180.88	223.04
3%	174.48	171.86	253.68

3. Mohammad Rakibul Islam
4. A. N. M. Iftekher
5. Md Sanowar Hosen
6. Mhamud Hasan Mim
7. Mirza Muntasir Nishat

Funding

The funding for this research was provided by the Islamic University of Technology, located in Dhaka, Gazipur 1704, Bangladesh, under the title “IUT Seed Grant.” The grant number for this project is REASP/IUT-RSG/2022/OL/07/009.

CRediT authorship contribution statement

Atiqul Alam Chowdhury: Writing – review & editing, Writing – original draft, Software, Formal analysis. **Md Rezaul Hoque Khan:** Validation, Supervision, Conceptualization. **Mohammad Rakibul Islam:** Visualization, Validation, Resources. **A.N.M. Iftekher:** Writing – review & editing, Validation. **Md Sanowar Hosen:** Writing – review & editing, Data curation. **Mhamud Hasan Mim:** Writing – review & editing, Resources. **Mirza Muntasir Nishat:** Methodology, Investigation.

Declaration of competing interest

The author declared no conflict of interest.

Data availability

Data will be made available on request.

References

[1] M.R.H. Khan, F.A.M. Ali, M.R. Islam, Thz sensing of covid-19 disinfecting products using photonic crystal fiber, Sens. Bio-Sens. Res. 33 (2021) 100447.
[2] A.A. Chowdhury, M.R.H. Khan, M.I.H. Bhuiyan, M.R. Islam, M.M. Nishat, et al., Highly sensitive pcf-spr biosensor for glioblastoma brain cancer detection, in: 2023 IEEE Photonics Conference (IPC), IEEE, 2023, pp. 1–2.
[3] M.R.H. Khan, M.S. Hosen, A.A. Chowdhury, M.R. Islam, F. Faisal, M.M. Nishat, N.I. B. Hamid, Silicate-glass based photonic crystal fiber for rapid petro-chemical sensing: design and analysis, Sens. Bio-Sens. Res. 100579 (2023).
[4] M.R.H. Khan, A.A. Chowdhury, M.R. Islam, M.S. Hosen, M.H. Mim, M.M. Nishat, Wave-shaped microstructure cancer detection sensor in terahertz band: design and analysis, Appl. Sci. 13 (9) (2023) 5784.
[5] M.R. Islam, A. Iftekher, M.H.I. Meraz, M.J. Nayen, M.R.H. Khan, Design of a dual arrow shaped and dual plasmonic material compatible spr pcf sensor, Opt. Quant. Electron. 55 (13) (2023) 1125.
[6] M.R. Islam, A.M.A. Naser, F.Z. Jaba, F. Anzum, A.N.M. Iftekher, M.R.H. Khan, M. M. Nishat, Design of a hexagonal outlined porous cladding with vacant core photonic crystal fibre biosensor for cyanide detection at thz regime, IET Optoelectron. 16 (4) (2022) 160–173.
[7] M.R. Islam, F. Yasir, M.R.H. Antor, M.H. Turja, A. Rahman, M.R.H. Khan, M. T. Reza, An eye-shaped ultra-sensitive localized surface plasmon resonance–based biochemical sensor, Plasmonics (2021) 1–11.

[8] M.R. Islam, A. Iftekher, F. Noor, M.R.H. Khan, M. Reza, M.M. Nishat, et al., Azo-coated plasmonic pcf nanosensor for blood constituent detection in near-infrared and visible spectrum, Appl. Phys. A Mater. Sci. Process. 128 (1) (2022) 1–13.

[9] C. Chen, J. Wang, Optical biosensors: an exhaustive and comprehensive review, Analyst 145 (5) (2020) 1605–1628.

[10] Y.-T. Chen, Y.-C. Lee, Y.-H. Lai, J.-C. Lim, N.-T. Huang, C.-T. Lin, J.-J. Huang, Review of integrated optical biosensors for point-of-care applications, Biosensors 10 (12) (2020) 209.

[11] A. Tereshchenko, M. Bechelany, R. Viter, V. Khranovskyy, V. Smyntyna, N. Starodub, R. Yakimova, Optical biosensors based on zno nanostructures: advantages and perspectives. A review, Sensors Actuators B Chem. 229 (2016) 664–677.

[12] H.F. Fakhruldeen, A.Z. Zahid, R.M. Jaafar, A. Abdulkareem, An overview of photonic crystal fiber (pcf), Indian J. Nat. Sci. 9 (53) (2019) 0976–0997.

[13] M.S. Islam, J. Sultana, M. Faisal, M.R. Islam, A. Dinovitser, B.W. Ng, D. Abbott, A modified hexagonal photonic crystal fiber for terahertz applications, Opt. Mater. 79 (2018) 336–339.

[14] H. Ademgil, S. Haxha, Pcf based sensor with high sensitivity, high birefringence and low confinement losses for liquid analyte sensing applications, Sensors 15 (12) (2015) 31833–31842.

[15] R. Lanza, J. Gearhart, B. Hogan, D. Melton, R. Pedersen, E.D. Thomas, J. A. Thomson, Essentials of Stem Cell Biology, Elsevier, 2005.

[16] H. Sung, J. Ferlay, R.L. Siegel, M. Laversanne, I. Soerjomataram, A. Jemal, F. Bray, Global cancer statistics 2020: Globocan estimates of incidence and mortality worldwide for 36 cancers in 185 countries, CA Cancer J. Clin. 71 (3) (2021) 209–249.

[17] D. Rodriguez-Abreu, A. Bordoni, E. Zucca, Epidemiology of hematological malignancies, Ann. Oncol. 18 (2007) i3–i8.

[18] R.L. Bertholf, Disorders of the adrenal gland, in: Handbook of Diagnostic Endocrinology, Elsevier, 2021, pp. 103–156.

[19] G.N. Sharma, R. Dave, J. Sanadya, P. Sharma, K. Sharma, Various types and management of breast cancer: an overview, J. Adv. Pharm. Technol. Res. 1 (2) (2010) 109.

[20] E. Dika, F. Scarfì, M. Ferracin, E. Broseghini, E. Marcelli, B. Bortolani, E. Campione, M. Riefolo, C. Ricci, M. Lambertini, Basal cell carcinoma: a comprehensive review, Int. J. Mol. Sci. 21 (15) (2020) 5572.

[21] K.S. Okunade, Human papillomavirus and cervical cancer, J. Obstet. Gynaecol. 40 (5) (2020) 602–608.

[22] L.H. Einhorn, Testicular cancer as a model for a curable neoplasm: the richard and hinda rosenthal foundation award lecture, Cancer Res. 41 (9_Part_1) (1981) 3275–3280.

[23] J. Cuzick, T. Powles, U. Veronesi, J. Forbes, R. Edwards, S. Ashley, P. Boyle, Overview of the main outcomes in breast-cancer prevention trials, Lancet 361 (9354) (2003) 296–300.

[24] G.E. Dressing, P. Thomas, Identification of membrane progestin receptors in human breast cancer cell lines and biopsies and their potential involvement in breast cancer, Steroids 72 (2) (2007) 111–116.

[25] K. Tajima, Y. Obata, H. Tamaki, M. Yoshida, Y.-T. Chen, M.J. Scanlan, L.J. Old, H. Kuwano, T. Takahashi, T. Takahashi, et al., Expression of cancer/testis (ct) antigens in lung cancer, Lung Cancer 42 (1) (2003) 23–33.

[26] K. Glunde, Z.M. Bhujwalla, Metabolic tumor imaging using magnetic resonance spectroscopy, in: Seminars in Oncology vol. 38, Elsevier, 2011, pp. 26–41.

[27] Y. Furusawa, Y. Fujiwara, P. Campbell, Q.-L. Zhao, R. Ogawa, M. Ali Hassan, Y. Tabuchi, I. Takasaki, A. Takahashi, T. Kondo, Dna double-strand breaks induced by cavitational mechanical effects of ultrasound in cancer cell lines, PLoS One 7 (1) (2012) e29012.

[28] W. Weber, S. McCarthy, Surface-plasmon resonance as a sensitive optical probe of metal-film properties, Phys. Rev. B 12 (12) (1975) 5643.

[29] M. De, T.K. Gangopadhyay, V.K. Singh, Prospects of photonic crystal fiber as physical sensor: an overview, Sensors 19 (3) (2019) 464.

[30] R. Otupiri, E.K. Akowuah, S. Haxha, Multi-channel spr biosensor based on pcf for multi-analyte sensing applications, Opt. Express 23 (12) (2015) 15716–15727.

[31] D. Rajeswari, A.A. Revathi, Highly sensitive spr-based pcf bio sensor for plasma cell detection in human blood for the detection of early stage cancer, Optik 258 (2022) 168897.

[32] Y. Gamal, B. Younis, A.E.-S. Abd-Elkader, D. Furniss, M. Farries, S. Phang, T. M. Benson, A.B. Seddon, M.F.O. Hameed, S. Obayya, Mid-infrared water pollutant sensor based on spr-pcf, Opt. Quant. Electron. 55 (11) (2023) 966.

[33] A. Rifat, G.A. Mahdiraji, Y. Sua, Y. Shee, R. Ahmed, D.M. Chow, F.M. Adikan, Surface plasmon resonance photonic crystal fiber biosensor: a practical sensing approach, IEEE Photon. Technol. Lett. 27 (15) (2015) 1628–1631.

[34] S. Mittal, A. Saharia, Y. Ismail, F. Petruccione, A.V. Bourdine, O.G. Morozov, V. V. Demidov, J. Yin, G. Singh, M. Tiwari, Spiral shaped photonic crystal fiber-based surface plasmon resonance biosensor for cancer cell detection, Photonics 10 (2023) 230. MDPI.

[35] M.S. Karim, S. Hossin, M.R. Alam, M.A.B. Siddik, M.R. Aktar, N. Ahmed, M.A. N. Shakh, Quad core gold coated photonic crystal fiber temperature sensor based on surface plasmon resonance, Sens. Bio-Sens. Res. 39 (2023) 100548.

[36] A. Yasli, Cancer detection with surface plasmon resonance-based photonic crystal fiber biosensor, Plasmonics 16 (2021) 1605–1612.

[37] A. Ehyaee, M. Mohammadi, M. Seifouri, S. Olyaee, Design and numerical investigation of a dual-core photonic crystal fiber refractive index sensor for cancer cells detection, Europ. Phys. J. Plus 138 (2) (2023) 129.

[38] V. S. Chaudhary, D. Kumar, S. Kumar, Au-tio 2 coated photonic crystal fiber based spr refractometric sensor for detection of cancerous cells, IEEE Trans. Nanobiosci.

[39] M.R. Sardar, M. Faisal, Dual-core dual-polished PCF-SPR sensor for cancer cell detection, IEEE Sensors J. (2024).

[40] M. Abdelghaffar, Y. Gamal, R.A. El-Khoribi, W. Soliman, Y. Badr, M.F.O. Hameed, S. Obayya, Cancer cell detection by plasmonic dual v-shaped PCF biosensor, JOSA B 41 (1) (2024) 222–229.

[41] K.M. Ibrahimi, R. Kumar, W. Pakhira, Enhance the design and performance analysis of a highly sensitive twin-core pcf spr biosensor with gold plating for the early detection of cancer cells, Plasmonics 18 (3) (2023) 995–1006.

[42] X. Yang, S. Hou, C. Xie, G. Wu, Z. Yan, High-performance photonic crystal fiber biosensor based on surface plasmon resonance for early cancer detection, Plasmonics (2023) 1–11.

[43] D.J.J. Hu, H.P. Ho, Recent advances in plasmonic photonic crystal fibers: design, fabrication and applications, Adv. Opt. Photon. 9 (2) (2017) 257–314.

[44] A. Matikainen, T. Nuutinen, T. Itkonen, S. Heinilehto, J. Puustinen, J. Hiltunen, J. Lappalainen, P. Karioja, P. Vahimaa, Atmospheric oxidation and carbon contamination of silver and its effect on surface-enhanced raman spectroscopy (Sers), Sci. Rep. 6 (1) (2016) 37192.

[45] Y. Chen, Y. Yu, X. Li, Z. Tan, Y. Geng, Experimental comparison of fiber-optic surface plasmon resonance sensors with multi metal layers and single silver or gold layer, Plasmonics 10 (2015) 1801–1808.

[46] P. Ambhorkar, Z. Wang, H. Ko, S. Lee, K.-I. Koo, K. Kim, D.-I. Cho, Nanowire-based biosensors: from growth to applications, Micromachines 9 (12) (2018) 679.

[47] E.K. Akowuah, T. Gorman, H. Ademgil, S. Haxha, G.K. Robinson, J.V. Oliver, Numerical analysis of a photonic crystal fiber for biosensing applications, IEEE J. Quantum Electron. 48 (11) (2012) 1403–1410.

[48] A. Vial, A.-S. Grimault, D. Macías, D. Barchiesi, M.L. De La Chapelle, Improved analytical fit of gold dispersion: application to the modeling of extinction spectra with a finite-difference time-domain method, Phys. Rev. B 71 (8) (2005) 085416.

[49] H. Assi, Time-Domain Modeling of Elastic and Acoustic Wave Propagation in Unbounded Media, with Application to Metamaterials, University of Toronto (Canada), 2016.

[50] A. Chen, F. Heismann, Polarization control, in: Encyclopedic Handbook of Integrated Optics, CRC Press, 2018, pp. 306–318.

[51] Z. Lin, S. Chen, C. Lin, Sensitivity improvement of a surface plasmon resonance sensor based on two-dimensional materials hybrid structure in visible region: a theoretical study, Sensors 20 (9) (2020) 2445.

[52] M.M. Hossain, M. Maniruzzaman, Study of confinement loss in photonic crystal fiber, in: International Conference on Materials, Electronics & Information Engineering, 2015.

[53] M.R. Islam, A. Iftekhar, A.A. Hassan, S. Zaman, M.A. Al Hosain, Double plasmonic peak shift sensitivity: an analysis of a highly sensitive lspr-pcf sensor for a diverse range of analyte detection, Appl. Phys. A Mater. Sci. Process. 129 (8) (2023) 571.

[54] A. Pathak, B. Rahman, C. Viphavakit, Nanowire embedded micro-drilled dual-channel approach to develop highly sensitive biosensor, IEEE Photon. Technol. Lett. 34 (13) (2022) 707–710.

[55] M. Quan, J. Tian, Y. Yao, Ultra-high sensitivity fabry–perot interferometer gas refractive index fiber sensor based on photonic crystal fiber and Vernier effect, Opt. Lett. 40 (21) (2015) 4891–4894.

[56] L. Xu, C. Peng, T. Meng, Y. Shi, Q. Liu, J. Lv, W. Liu, P.K. Chu, C. Liu, High-sensitivity ring-core photonic crystal fiber sensor based on surface plasmon resonance for ultra-low refractive index detection, Mod. Phys. Lett. B 38 (02) (2024) 2350216.

[57] E. Haque, A. Al Noman, M.A. Hossain, N.H. Hai, Y. Namihira, F. Ahmed, Highly sensitive d-shaped plasmonic refractive index sensor for a broad range of refractive index detection, IEEE Photon. J. 13 (1) (2021) 1–11.

[58] M.A. Jabin, K. Ahmed, M.J. Rana, B.K. Paul, M. Islam, D. Vigneswaran, M.S. Uddin, Surface plasmon resonance based titanium coated biosensor for cancer cell detection, IEEE Photon. J. 11 (4) (2019) 1–10.

[59] M.H. Pappu, A. Rahman, M.A. Mollah, An h-shaped exposed core surface plasmon resonance sensor and detection of cancer cells, Plasmonics (2024) 1–17.

[60] S. Singh, B. Chaudhary, A. Upadhyay, S.A. Taya, Bottom side partially etched d-shaped pcf biosensor for early diagnosis of cancer cells, Europ. Phys. J. Plus 138 (6) (2023) 511.

[61] H. El Hamzaoui, Y. Ouerdane, L. Bigot, G. Bouwmans, B. Capoen, A. Boukenter, S. Girard, M. Bouazaoui, Sol-gel derived ionic copper-doped microstructured optical fiber: a potential selective ultraviolet radiation dosimeter, Opt. Express 20 (28) (2012) 29751–29760.

[62] B. Dabas, R. Sinha, Dispersion characteristic of hexagonal and square lattice chalcogenide as2se3 glass photonic crystal fiber, Opt. Commun. 283 (7) (2010) 1331–1337.

[63] V.R.K. Kumar, A. George, W. Reeves, J. Knight, P.S.J. Russell, F. Omenetto, A. Taylor, Extruded soft glass photonic crystal fiber for ultrabroad supercontinuum generation, Opt. Express 10 (25) (2002) 1520–1525.

[64] M. El-Amraoui, G. Gadret, J. Jules, J. Fatome, C. Fortier, F. Désévédavy, I. Skripatchev, Y. Messaddeq, J. Troles, L. Brilland, et al., Microstructured chalcogenide optical fibers from as 2 s 3 glass: towards new ir broadband sources, Opt. Express 18 (25) (2010) 26655–26665.

[65] W. Talataisong, R. Ismaeel, S.R. Sandoghchi, T. Rutirawut, G. Topley, M. Beresna, G. Brambilla, Novel method for manufacturing optical fiber: extrusion and drawing of microstructured polymer optical fibers from a 3d printer, Opt. Express 26 (24) (2018) 32007–32013.

[66] S. Atakaramians, S. Afshar, H. Ebendorff-Heidepriem, M. Nagel, B.M. Fischer, D. Abbott, T.M. Monro, Thz porous fibers: design, fabrication and experimental characterization, Opt. Express 17 (16) (2009) 14053–14062.

[67] Z. Liu, H.-Y. Tam, Fabrication and sensing applications of special microstructured optical fibers, in: F. Xu, C. Mou (Eds.), Selected Topics on Optical Fiber Technologies and Applications, 2017, pp. 1–20.
[68] D. Pysz, I. Kujawa, R. Stepień, M. Klimczak, A. Filipkowski, M. Franczyk, L. Kociszewski, J. Buźniak, K. Haraśny, R. Buczyński, Stack and draw fabrication of soft glass microstructured fiber optics, Bull. Pol. Academy Sci. Techn. Sci. 62 (4).
[69] A.L. Cruz, C. Cordeiro, M.A. Franco, 3d printed hollow-core terahertz fibers, Fibers 6 (3) (2018) 43.
[70] J. Zhang, J. Yuan, Y. Qu, S. Qiu, C. Mei, X. Zhou, B. Yan, Q. Wu, K. Wang, X. Sang, et al., A surface plasmon resonance-based photonic crystal fiber sensor for simultaneously measuring the refractive index and temperature, Polymers 14 (18) (2022) 3893.
[71] M. Rezapour Sarabi, S.A. Nakhjavani, S. Tasoglu, 3d-printed microneedles for point-of-care biosensing applications, Micromachines 13 (7) (2022) 1099.
[72] E. Sokullu, Z.L. Cücük, M.R. Sarabi, M.T. Birtek, H.S. Bagheri, S. Tasoglu, Microfluidic invasion chemotaxis platform for 3d neurovascular co-culture, Fluids 7 (7) (2022) 238.